Efficiency correction factors in whole body counting due to the biodistribution of radionuclides

J. Bento[1]*, S. Barros[1], P. Teles[1], P. Vaz[1], M. Zankl[2]

[1]Instituto Tecnológico e Nuclear, Instituto Superior Técnico, Universidade Técnica de Lisboa, Estrada Nacional 10, 2686-953 Sacavém, Portugal
[2]Helmholtz Zentrum München, Ingolstädter Landstraße 1, 85764 Neuherberg, Germany

* Corresponding author. Tel.: +351 21 994 6334; fax: +351 21 994 1995.
E-mail address: joana.bento@itn.pt (J. Bento)

Abstract

The efficiency calibration of whole body counters for monitoring of internal contaminations is usually performed with anthropomorphic physical phantoms assuming homogeneous activity distribution. Besides the inherent limitations of these phantoms in resembling the human anatomy, they do not represent a realistic activity distribution, since in real situations each incorporated radionuclide has its particular biodistribution after entering the systemic circulation. Moreover, the activity content in the different organs and tissues comprising the biokinetics is time dependent. This work aims at assessing the whole body counting efficiency deviations arising from considering a detailed voxel phantom instead of a standard physical phantom (BOMAB) and at evaluating the effect of the anatomical differences between both phantoms. It also aims at studying the efficiency considering the biodistribution of a set of radionuclides of interest incorporated in the scope of environmental and occupational exposures (inhalation and ingestion) and at computing the time-dependent efficiency correction factors to account for the biodistribution variation over time. For the purpose, Monte Carlo simulations were performed to simulate the whole body counting efficiencies and biokinetic models were used to estimate the radionuclides´ biokinetic behaviour in the human body after intake. The comparison between the efficiencies obtained with BOMAB and the voxel phantom showed deviations between 1.8% and 11.7%, proving the adequacy of the BOMAB for whole body counter calibration. The obtained correction factors show that the effect of the biodistribution in the whole body counting efficiency is more pronounced in cases of acute activity uptake and long term retention in certain organs (3-89%) than in cases of homogeneous distribution in body tissues (1-8%), for which the biokinetics influence can be neglected. This work further proves the powerful combination of Monte Carlo simulation methods using voxel phantoms and biokinetic models for internal dosimetry studies.

Keywords (max 6)

Whole body counter, Monte Carlo simulations, BOMAB phantom, Voxel phantoms, Biokinetic models

1. Introduction

The internal dose assessment requires an accurate quantification of the radioactivity incorporated in the human body by inhalation, ingestion or direct absorption thought skin. The accuracy of the *in vivo* measurement greatly depends on the similarity between the physical calibration phantom and the measured individual in terms of anatomy, attenuation properties and radioactive material distribution.

Radiation counters for whole body monitoring are commonly calibrated using the Bottle Manikin Absorption (BOMAB) phantom (ANSI, 1999) – a standard anthropomorphic physical phantom for whole body counters (WBC) (Kramer, 1991; Schläger, 2011) – consisting of water filled plastic cylindrical containers. Still, the BOMAB phantom presents some limitations in mimicking a contaminated individual, since it does not represent the realistic human body anatomy and does not take into account the internal organs. To evaluate the influence of the anatomical differences, Monte Carlo (MC) methods can be used to simulate whole body counting efficiencies using realistic human tomographic image-based models (voxel phantoms). Several studies (Kinase, 2007; Hunt, 2000; Franck, 2003; Moraleda, 2004; Genicot, 2008; Schlagbauer, 2007) have shown that MC simulations and voxel phantoms can be employed to estimate the accuracy of calibration procedures of *in vivo* monitoring systems and the associated uncertainties. Some authors (Zhang, 2008; Takahashi, 2010) performed comparative studies between BOMAB and voxel phantoms and have concluded that both phantoms can have similar whole body counting efficiencies if they have similar weight and mass.

A major limitation of the BOMAB phantom is related to the activity distribution, which is homogeneously distributed in the constituent containers in contrast with the biodistribution verified in a contaminated individual. As widely reported by the International Commission on Radiological Protection (ICRP) (ICRP, 1979; ICRP, 1980; ICRP, 1981; ICRP1990; ICRP, 1993; ICRP, 1995a), every element, or group of similar elements, has a different behaviour within the human body after entering the systemic circulation. Even for radionuclides assumed to be homogenously distributed in body tissues after entering the circulatory system, such as caesium isotopes, considerable amounts of the incorporated activity are retained in the respiratory tract and/or gastrointestinal tract contents countering the homogeneity assumption. Also, the incorporated activity is eliminated at different rates from the several organs and tissues involved in the biokinetics, making the biodistribution time dependent. Some studies (Carlan, 2007; Lamart, 2009) have shown significant discrepancies in efficiency when considering the radionuclides' biokinetics.

In this work, Monte Carlo simulations using the state-of-the-art computer program MCNPX were performed to simulate the WBC efficiency using a BOMAB phantom and a voxel phantom (assuming homogeneous activity distribution), in order to assess the influence of the anatomical discrepancies between both phantoms. To evaluate the effect of the activity biodistribution in the whole body counting efficiency, a computational study using Monte Carlo and biokinetics software was performed, taking into account the biokinetic models in several internal contamination scenarios. For environmental exposure, inhalation and ingestion of ^{131}I, ^{134}Cs and ^{137}Cs were considered; for the occupational exposure, inhalation and ingestion of ^{131}I, ^{60}Co and ^{137}Cs were the selected scenarios. The ratio between the efficiency considering the radionuclides biodistribution over time and the efficiency assuming activity homogeneously distributed for each contamination scenario was used to compute time-dependent correction factors for whole body counting efficiency. These correction factors were also used to optimise the monitoring programme in terms of the time schedule to perform the measurements and for uncertainty assessment, in the absence of corrected efficiency values.

2. Whole body counting efficiency

2.1 – Whole Body Counter

The WBC (ACCUSCAN II, Canberra) in operation at the Instituto Tecnológico e Nuclear (ITN) is a vertical scanning counter with a moving detector, including a 10 cm steel shielding mechanism for environmental background reduction. It integrates a p-type High-Purity Germanium detector (Coaxial Ge Detector GC 2520, Canberra) with a relative efficiency of 25%. The Germanium crystal (2.78 cm diameter and 4.75 cm length) is enclosed in a 1.5 mm thickness aluminium endcap; the detector shielding is made of a set of layers of different materials (0.3 mm copper, 44 mm lead and 0.2 mm iron). The detection range of this system varies from 50 keV to over 2000 keV.

2.2 – BOMAB Phantom

The BOMAB phantom consists of a collection of ten polyethylene (0.94 g cm^{-3} density) containers of circular and elliptical cross section, representing the head, neck, thorax, abdomen, arms, thighs and legs. The side wall thickness of the containers is 0.25cm; the top and bottom thicknesses are 2.3 cm and 0.9 cm, respectively.

The BOMAB phantom was filled with radioactive material in an acidified deionized water solution. A mixed radionuclide gamma-ray reference standard, consisting of nine radionuclides (^{109}Cd, ^{57}Co, ^{139}Ce, ^{203}Hg, ^{113}Sn, ^{85}Sr, ^{137}Cs, ^{60}Co and ^{88}Y) provided in a 5 ml ampoule, was distributed by the ten phantom pieces proportionally to their inner volume to ensure a homogeneous activity distribution. For positioning the BOMAB phantom in the WBC in the standing position, the phantom containers were piled in a medium density fibreboard (MDF) and wood support. The experimental setup for WBC calibration with the BOMAB phantom is shown in Figure 1.

Figure 1 – ACCUSCAN II whole body counter and the BOMAB phantom.

2.3 – Voxel Phantom

The Golem voxel phantom (Zankl, 2001), from the GSF Voxel Computational Phantom Family, was developed at Helmholtz Zentrum München, formerly GSF (National Research Center for Environment and Health), from tomographic image data of an adult male. Golem was segmented into 121 organs or tissues, containing nearly 1.9 million non-zero voxels, with a voxel resolution of 0.208 cm × 0.208 cm × 0.8 cm. The Golem structures consist of skin, muscle tissue, soft tissue, adipose tissue and lungs; the skeletal components consist of a mixture of mineral bone and bone marrow, with average density 1.45 g cm^{-3}.

The whole body counting efficiencies were simulated using the reference male BOMAB phantom and the Golem voxel phantom. The height, weight and whole body volume of both phantoms are displayed in Table 1.

	Phantom	
	BOMAB	**Golem**
Height (cm)	170	176
Weight (kg)	68.1	69
Volume (cm^3)	68275	67377

Table 1 - Height, weight and whole body volume of BOMAB and Golem.

2.4 – Determination of the WBC efficiency by Monte Carlo simulations

The WBC calibration with the BOMAB phantom and the corresponding Monte Carlo simulation using the programs MCNPX v.2.6.0 (McKinney, 2006) and PENELOPE v.2008 (Salvat, 2008) have already been reported (Bento, 2012). In this previous work, the implementation of the detector movement in the MC simulations was addressed, since a whole body measurement requires a scan along the subject length. An averaging method, previously proposed by Kramer et al (Kramer, 2002), was applied considering the detector at nine different positions along the BOMAB height. Deviations between experimental and computational efficiencies were found below 5%, validating the computational description of the experimental setup and the averaging method for calculating the computational whole body counting efficiencies.

However, the used averaging method was time-consuming, since it involved nine separate simulations. In this work, a new approach was tested, defining the detector at the nine positions simultaneously (using MCNPX Repeated Structures cards) and performing a single simulation. Comparing to the nine simulation method, this approach has shown to be faster and the deviations in the efficiency values were found below 4% in the whole energy range. Therefore, in the following simulations the single simulation method was used. The new efficiency values obtained for the BOMAB phantom using the single simulation method were used.

In this work, Monte Carlo simulations were performed to calculate whole body counting efficiencies with the Golem voxel phantom using MCNPX v.2.7.0 (McKinney, 2009). In order to reproduce the calibration with the BOMAB phantom conditions, Golem was placed in the same relative position and the activity distribution was defined homogeneously. For the purpose, all Golem organs and tissues were defined as the radiation source and the source distribution was defined proportionally to the number of voxels of each tissue composing the voxel phantom. The full energy peak efficiency was calculated using the MCNPX pulse-height tally (F8). The number of simulated particles ($1x10^8$) was selected to keep statistical uncertainties (k=1) below 2%.

The implemented computational models of the whole body counting setups with the BOMAB and Golem phantoms are shown in Figure 2.

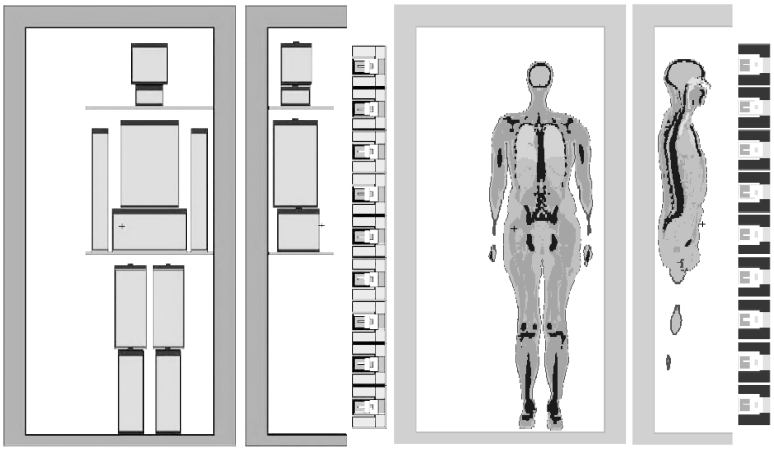

(a) (b) (c) (d)

Figure 2 – Computational whole body counting setups: front (a) and side (b) views of BOMAB phantom and front (c) and side (d) views of the Golem voxel phantom.

The whole body counting efficiencies obtained with BOMAB and Golem, using the single simulation method, are listed in Table 2, as well as the deviation between both values.

		Efficiency (cps/γ)		
Nuclide	**Energy**	**BOMAB**	**Golem**	**Relative Deviation**
^{109}Cd	88.04	7.81×10^{-5} (6.49%)	7.340×10^{-5} (0.15%)	-6.02%
^{57}Co	122.06	1.23×10^{-4} (2.24%)	1.205×10^{-4} (0.11%)	-2.01%
^{139}Ce	165.86	1.42×10^{-4} (1.87%)	1.259×10^{-4} (0.13%)	-11.35%
^{203}Hg	279.197	1.18×10^{-4} (1.63%)	1.046×10^{-4} (0.26%)	-11.38%
^{113}Sn	391.69	9.54×10^{-5} (4.04%)	8.613×10^{-5} (0.30%)	-9.72%
^{85}Sr	514.01	8.04×10^{-5} (1.69%)	7.522×10^{-5} (0.43%)	-6.44%
^{137}Cs	661.66	6.81×10^{-5} (1.65%)	6.351×10^{-5} (0.37%)	-6.74%
^{88}Y	898.04	5.83×10^{-5} (1.73%)	5.335×10^{-5} (0.66%)	-8.49%
^{60}Co	1173.24	5.09×10^{-5} (1.54%)	4.787×10^{-5} (0.50%)	-5.96%
^{60}Co	1332.5	4.66×10^{-5} (1.34%)	4.401×10^{-5} (0.53%)	-5.57%
^{88}Y	1836.06	3.82×10^{-5} (1.63%)	3.691×10^{-5} (0.80%)	-3.38%

Table 2 – Whole body counting efficiencies for BOMAB phantom and Golem voxel phantom.

The results show that the efficiencies for Golem voxel phantom are 2.0-11.4% lower than the reference male BOMAB phantom. These discrepancies were expected, since Golem is 1.3% heavier and 3.5% higher than BOMAB, causing greater photon attenuation. Thus, the adequacy of the BOMAB phantom for WBC calibration is enhanced, taking into account all the anatomical differences between the physical phantom and the voxel model.

3. Time-dependent correction factors accounting for the biodistribution

3.1 – Intake scenarios

To compute the time-dependent correction factors for the whole body counting efficiency resulting from the radionuclides' biodistribution, relevant internal contamination scenarios in the framework of environmental and occupational exposures were considered.

For environmental exposure, inhalation and ingestion of ^{131}I, ^{134}Cs and ^{137}Cs were considered. These radionuclides are the typical signature of radioactivity releases into the environment associated to nuclear accidents, as was the case after the Fukushima nuclear power plant accident (Masson, 2011) which releases were detected in the Iberian Peninsula sixteen days later (Lozano, 2011). For the occupational exposure, the intake scenarios correspond to the inhalation and ingestion of ^{131}I, ^{60}Co and ^{137}Cs, since these radionuclides are commonly considered in the framework of internal contamination following potential accidents during the activities of radiological installations and practices in the medical and industrial sectors as well as associated to nuclear reactors´ operation and maintenance.

3.2 – Biokinetic functions (DCAL)

The activity versus time functions in body compartments following the intake for all the contamination scenarios were estimated using DCAL (Dose and Risk Calculation software), version 8.4 (Eckerman, 2006). DCAL performs age-specific biokinetic and dosimetric calculations for acute intake of radionuclides by inhalation, ingestion and injection based on ICRP biokinetic models. In this work, the ACTACAL module was used to table activity fraction in each biokinetic model compartment over time after incorporation of 1Bq.

The deposition of inhaled particles is calculated for each region of the respiratory tract, which is represented by extrathoracic, bronchial, bronchiolar and alveolar-interstitial regions; lymphatic tissue is associated with both extrathoracic and thoracic regions (ICRP, 1994). The radionuclides may reach the gastrointestinal tract, represented by stomach, small intestine, upper large intestine and lower large intestine (ICRP, 1979a), directly by ingestion or indirectly by transfer from the respiratory tract or from other organs. After passing through the respiratory and/or gastrointestinal tracts, the radionuclide enters the systemic circulation and each element, or group of similar elements, has a characteristic systemic model.

It is assumed that 30% of iodine reaching the blood is accumulated in the thyroid and 70% is excreted by urine. The biological half time in blood is 0.25 days. Iodine leaves the thyroid with half-time of 80 days and enters other tissues where it is retained with a half-time of 12 days. Most of the iodine (80%) is subsequently released into the circulation for uptake by the thyroid and urinary excretion; the remaining 20% are excreted in faeces (ICRP, 1990).

Systemic caesium is taken to be distributed uniformly throughout all body tissues; 10% is assumed to be retained with biological-half time of 2 days and 90% with 110 days. The urinary to faecal excretion ratio is 4:1(ICRP, 1990).

Following the entry of cobalt into blood, 50% is rapidly excreted with half-time of 0.5 days, 5% is taken up by the liver and 45% is uniformly distributed in all other tissues. Fractions of 0.6, 0.2 and 0.2 are assumed to be lost from the liver and other tissues with biological half-time of 6, 60 and 800 days, respectively. The urinary to faecal excretion ratio is 6:1(ICRP, 1993).

In this work, all biokinetic functions were calculated for adult subjects. Concerning the inhalation cases, all radionuclides were considered to have fast uptake to body fluids (absorption type F), since this is the recommended default absorption type for particulate aerosols for public members (ICRP, 1995b) and workers (ICRP, 1994). Regarding the inhaled particles, activity median aerodynamic diameter (AMAD) aerosols of 1μm and 5μm were considered, since these are the recommended default AMAD values for environmental exposure (ICRP, 1995b) and occupational exposure (ICRP, 1994), respectively.

The biokinetic functions were generated, by default, from 0 to 365 days after the intake using increasing time steps. Given the effective half-life of the radionuclides involved in this study and the detection ability of *in vivo* monitoring techniques, this time interval was used to calculate the time-dependent correction factors for ^{134}Cs, ^{137}Cs and ^{60}Co but a shorter interval (0-180 days) was selected for ^{131}I.

3.3 – Monte Carlo Simulations

For each radionuclide, the efficiency was simulated for a single energy selected pondering the emission probability and the detector efficiency. Table 3 summarises the simulated radionuclides, selected energy and respective emission probability, the time interval used to calculate the time-dependent correction factors and the considered intake scenarios.

	Radionuclide			
	I-131	**Cs-134**	**Cs-137**	**Co-60**
$T_{1/2phys}$	8.0207 d	2.0648 y	30.07 y	5.2714 y
Energy	364.489 keV	604.721 keV	661.657 keV	1173.237 keV
Emission prob.	81.7%	97.62%	85%	99.97%
Time interval	0-180 d	0-365 d	0-365 d	0-365 d
Intake scenarios	Inhalation (Env.) Inhalation (Occu.) Ingestion	Inhalation (Env.) Ingestion	Inhalation (Env.) Inhalation (Occu.) Ingestion	Inhalation (Occu.) Ingestion

Table 3 – Simulated radionuclides, time intervals used to calculate the time-dependent correction factors and selected intake scenarios.

Initially, the WBC efficiency was simulated considering homogeneous activity distribution in the Golem voxel phantom for further calculations of correction factors due to the biodistribution. To assure statistical uncertainties below 1% (k=1), $5x10^7$ particles were simulated. The results are shown in Table 4.

Radionuclide	**Energy (keV)**	**Efficiency (cps/γ)**	**Uncertainty**
^{131}I	364.489	8.784E-05	0.81%
^{134}Cs	604.721	6.403E-05	0.95%
^{137}Cs	661.657	6.351E-05	0.37%
^{60}Co	1173.237	4.787E-05	0.50%

Table 4 – Whole body counting efficiencies considering activity homogeneously distributed.

To simulate the whole body counting efficiency taking into account the biodistribution, the organs and tissues comprised in the biokinetic model were defined as the radiation source in the Golem voxel phantom. As the activity fraction in each compartment is time dependent and variable between the several intake scenarios, the full energy peak efficiency was simulated for each organ separately and the results were then folded with the biokinetic functions estimated with DCAL for every intake scenario, in order to calculate the efficiency as function of the biodistribution. The number of simulated particles was selected according to the organs and tissues volume to assure statistical uncertainties (k=1) below 1%.

The DCAL biokinetic functions provide activity fractions for every compartment comprising the biokinetic models, including compartments of the respiratory tract, gastrointestinal tract and element-specific systemic model. However, not every compartment included in the biokinetic models has an exact corresponding structure at the Golem voxel phantom and some approximations had to be performed. Some organs are not segmented in such detail and others don't even exist, thus, the activity content in such organs had to be integrated in the existing Golem structures or ignored, if the activity content is negligible. In the absence of blood in the Golem structures, mainly due to the voxel resolution, the blood activity content was assumed to be homogeneously distributed into the body tissues (muscle tissue, adipose tissue and soft tissue). The DCAL biokinetic compartments and the corresponding Golem structures are listed in Table 5.

DCAL compartments	Golem organ or tissue
Respiratory tract	
Alveolar-interstitial region (AI)	Lungs
Bronchiolar region (bb)	
Bronchial region (BB)	Bronchial tree
Extra-thoracic airways: anterior nasal passage (ET1)	Anterior nasal passage
Extra-thoracic airways: posterior nasal passage, oral passage, pharynx and larynx (ET2)	Posterial nasal passage + pharynx + larynx
Lymphatic nodes	Not defined (negligible contribution)
Gastrointestinal tract	
Stomach content	Stomach content
Small intestine content	Small intestine (wall+content)
Upper large intestine content	Large intestine content
Lower large intestine content	
Excretion	
Urinary bladder content	Bladder content
Systemic models	
Blood	Muscle tissue + Adipose tissue + Soft tissue
Tissue	Muscle tissue + Adipose tissue + Soft tissue
Thyroid	Thyroid
Liver	Liver

Table 5 - DCAL biokinetic compartments and the corresponding Golem structures.

3.4 – Time-dependent correction factors

The calculated correction factors are the ratio between the efficiencies obtained considering the biodistribution over time and the efficiencies found considering homogeneous distribution listed in Table 4. The correction factors can be applied to whole body counting efficiency obtained with homogeneous distribution in order to cancel the biodistribution influence in the intake assessment or can be used to estimate the uncertainty associated to the disregarding of the biokinetics in the WBC calibration. Additionally, the time-dependent correction factor curve can be used to optimise the monitoring programme, allowing the selection of the most appropriate measuring times which are associated to minor errors related to biokinetics.

Figures 3 through 6 show, on the left, the correction factors calculated for the considered intake scenarios and, on the right, the biokinetic behaviour of the respective radionuclide after entering the systemic circulation. The biokinetic plots consider the sum of tissue and blood contributions to follow the same

method employed in the Monte Carlo simulations and show the urinary bladder content, since urine is the major route of excretion in the considered incorporation scenarios.

For all radionuclides in the study, the correction factors obtained for the three incorporation possibilities (environmental and occupational inhalation and ingestion) become equal after a time interval ranging from one day up to ten days, depending on the radionuclide. This radionuclide dependent equality occurs for the time at which the radioactive content in the respiratory tract and gastrointestinal tracts' compartments is null and only the compartments from the systemic models contribute to the biodistribution.

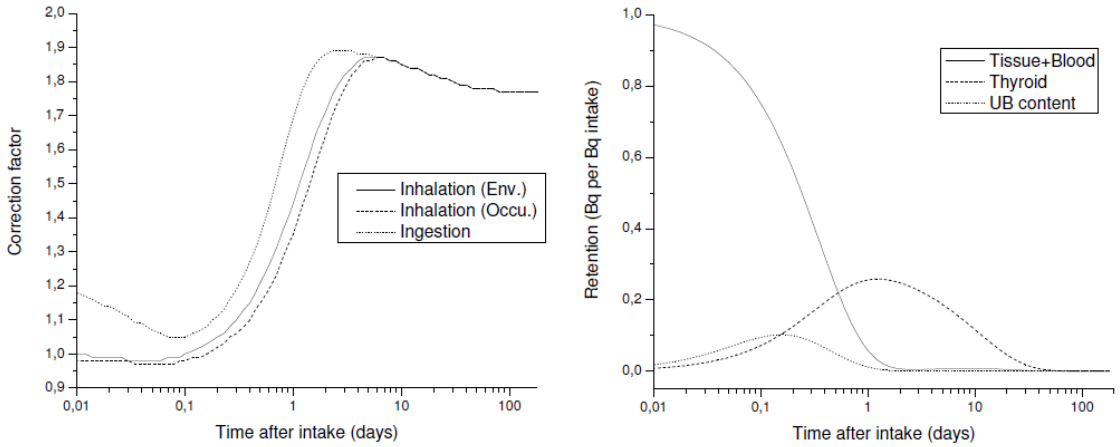

Figure 3 – Efficiency correction factors as a function of time after intake for incorporation of ^{131}I (left) and corresponding biokinetic functions (right).

The correction factors for intake of ^{131}I vary from 0.97 to 1.89, demonstrating a great influence of the biodistribution of ^{131}I in the whole body counting efficiency. The largest discrepancies are noticeable during the first 10 days following the intake, the most appropriate period for monitoring, taking into account the biokinetics and the detection capability of the *in vivo* detection systems. The correction factors reach a constant value (1.77) for both inhalation and ingestion 80 days after the intake.

These results show that the *in vivo* monitoring of ^{131}I in the time period 1-10 days after inhalation or ingestion, using a calibration that assumes homogeneous activity distribution, would result in 35-89% error in the activity quantification. If the biodistribution correction factors are not applied, the ^{131}I monitoring would be more accurate if performed by means of *in vivo* thyroid monitoring, which disregards any biodistribution influence, and/or urine measurements.

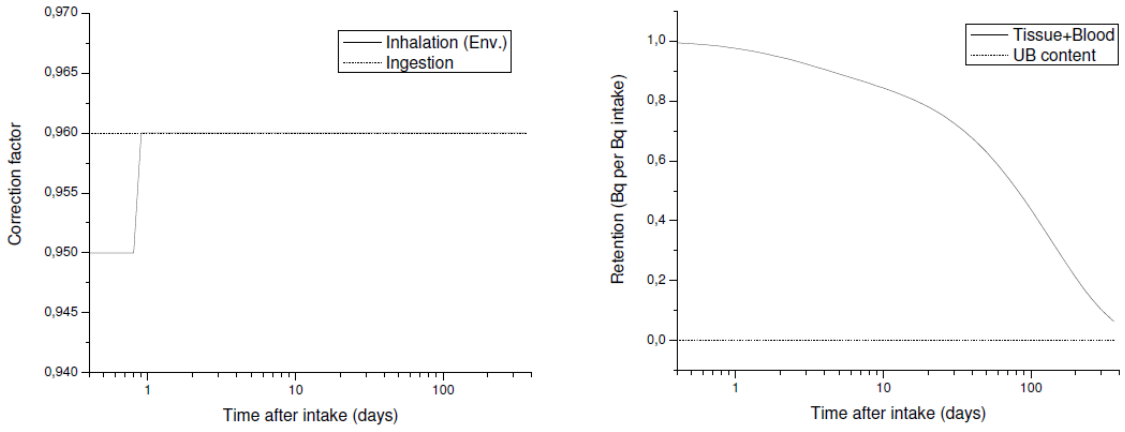

Figure 4 – Efficiency correction factors as a function of time after intake for incorporation of ^{134}Cs (left) and corresponding biokinetic functions (right).

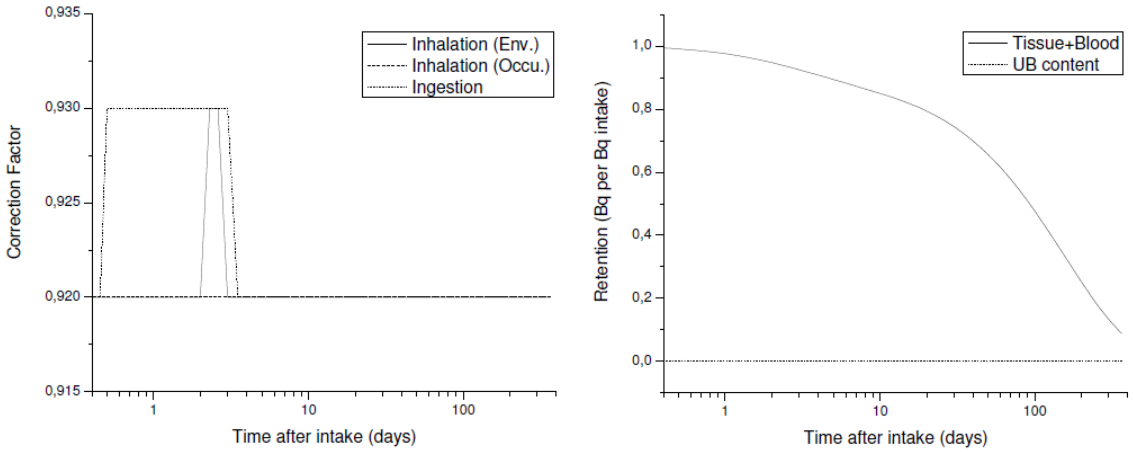

Figure 5 – Efficiency correction factors as a function of time after intake for incorporation of ^{137}Cs (left) and corresponding biokinetic functions (right).

Regarding the Caesium intakes, the correction fractions range between 0.95 and 0.96 for ^{134}Cs and between 0.92 and 0.93 for ^{137}Cs. Since after entering the circulation the Caesium isotopes are taken to be distributed uniformly through all body tissues, the biodistribution has a smaller influence in the whole body counting efficiency. For all routes of intake, the correction factors become constant approximately one day after ^{134}Cs intake (0.96) and approximately four days after ^{137}Cs incorporation (0.92).

The results suggest that *in vivo* whole body measurements are adequate for Caesium monitoring, even if WBC is calibrated assuming homogeneous activity distribution, since errors associated to activity quantification would be 4-5% for ^{134}Cs and 7-8% for ^{137}Cs. The biokinetics show that after 365 days following the intake, about 7% of the incorporated ^{134}Cs and about 9% of the incorporated ^{137}Cs are still retained in the whole body tissues. Thus, depending on the amount of incorporated activity and minimum detectable activity of the detection system, the measurements can be performed until one year after the internal contamination with acceptable errors associated to biodistribution.

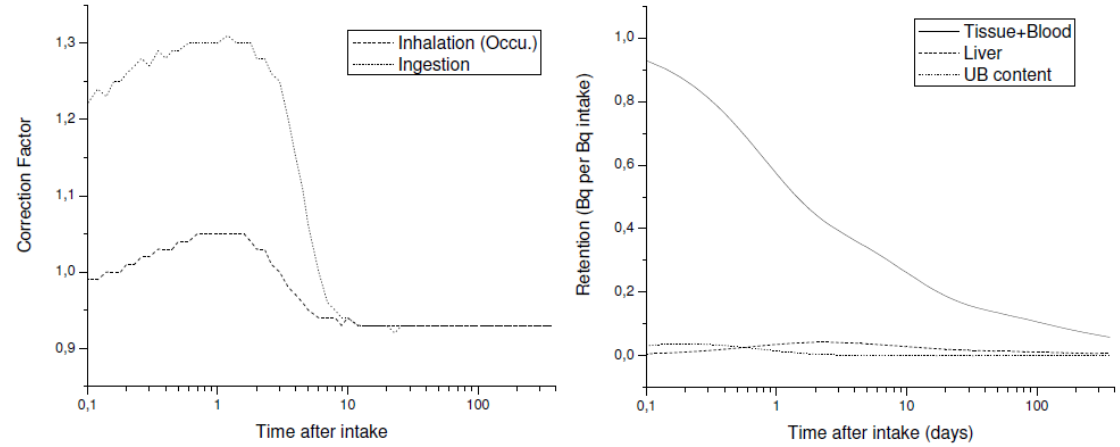

Figure 6 – Efficiency correction factors as a function of time after intake for incorporation of ^{60}Co (left) and corresponding biokinetic functions (right).

The correction factors values for incorporation of ^{60}Co also demonstrate the influence of the biodistribution, which is clearer in the first ten days after the intake. However, the correction factor in the whole body counting efficiency is much more pronounced in the case of ingestion than inhalation. For inhalation, the correction factor varies from 0.93 to 1.05 whereas for ingestion it ranges between 0.92 and 1.31; ten days after the incorporation, the correction factors achieve a constant value (0.93).

These results suggest that the whole body monitoring of ^{60}Co inhalation cases can be adequately performed with a WBC calibrated assuming homogenous activity distribution immediately after the

contamination, since errors associated with the biodistribution (5-7%) are acceptable. In the case on ^{60}Co ingestion, if correction factors are not applied to efficiency, the whole body measurements should be preferably performed at least 4.5 days after the intake, in order to assure an error associated to biodistribution below 10%. The biokinetics show that 4.5 days after the intake, about 40% of the incorporated ^{60}Co is still retained in the whole body tissues (including liver) and can certainly be detected by the *in vivo* monitoring equipment.

4. Conclusion

This work confirms the adequacy of the BOMAB phantom for WBC calibration, given its comparable performance when compared to a detailed voxel phantom. However, the calibration with the BOMAB phantom family is crucial for an accurate intake assessment, when measuring individuals with different heights and weights. Future work will consist on computing the efficiencies using the BOMAB phantom family in order to determine efficiency curves as function of height and weight.

The biodistribution of the radionuclides after incorporation has proven to influence the whole body counting efficiencies. The ratio between the efficiencies simulated considering the biodistribution and considering a homogeneous distribution was used to calculate correction factors to assess the influence of the biokinetics but has also proven to be useful in the optimisation and determination of the effectiveness of the internal monitoring programme. The results have shown that, in the absence of correction factors application, ^{131}I whole body monitoring is not very adequate, giving the large associated errors; ^{134}Cs and ^{137}Cs monitoring can be performed immediately after the contamination, since associated errors are acceptable and approximately time constant; ^{60}Co whole body monitoring is suitable if optimised in terms of the measuring time.

This work suggests that the biodistribution causes greater effect in the whole body counting efficiency in the cases of significant activity uptake and long term retention in certain organs, such as the thyroid after iodine intake. If the uptake in body organs is minor, such as liver uptake after Cobalt incorporation, the biokinetics will be less influent. Also, if the activity is assumed to be homogeneously distributed in body tissues after entering the circulation, like Caesium isotopes, the biodistribution effect can be neglected, since it leads to acceptable errors in the intake assessment.

It should be noted that the correction factors obtained relate to a whole body scanning detection system and they could significantly differ in the case of different monitoring geometries such as static detectors.

Last but not least, the methodology adopted in the work performed highlights the powerful combination of Monte Carlo simulations using voxel phantoms with biokinetic models, for internal dosimetry purposes and studies.

Acknowledgements

The authors would like to thank Fundação para a Ciência e a Tecnologia for Joana Bento's grant (SFRH/BI/33656/2009).

References

American National Standards Institute, 1999. Specifications for the Bottle Manikin Absorption Phantom, HPS N13.35

Bento J., Barros S., Teles P., Neves M., Gonçalves I., Vaz P., 2012. Monte Carlo simulation of the movement and detection efficiency of a Whole Body Counting system using a BOMAB Phantom. Radiat. Prot. Dosim. 148(4), 403-413

Carlan L, Roch P, Blanchardon E and Franck D, 2007 Application of voxel phantoms in whole-body counting for the validation of calibration phantoms and the assessment of uncertainties Radiat. Prot. Dosim. 125(1–4) 477–82

Eckerman K F, Leggett R W, Cristy M, Nelson C B, Ryman J C, Sjoreen A L and Ward R C, 2006. User's guide to the DCAL system Report No. ORNL/TM-2001/190 (Oak Ridge, TN: Oak Ridge National Laboratory)

Franck, D., Borissov, N., de Carlan, L., Pierrat, N., Genicot, J. L. and Etherington, G., 2003. Application of Monte Carlo calculations to calibration of anthropomorphic phantoms used for activity assessment of actinides in lungs. Radiat. Prot. Dosim. 105(1–4), 403–408

Genicot, J. L., Koukouliou, V. and Carinou, E., 2008. Monte Carlo calculations applied to the parametrical studies in a whole body counter. Radiat. Prot. Dosim. 128, 49 – 61

Hunt J.G, Malátová I, Foltánová S, Dantas B.M, 2000. Calibration of in vivo measurement system using a voxel phantom and the Monte Carlo technique. Radiat. Prot. Dosim. 89(3-4), 283-286

ICRP, 1979a. Limits for Intakes of Radionuclides by Workers. ICRP Publication 30 (Part 1). Ann. ICRP 2 (3-4).

ICRP, 1979b. Limits for Intakes of Radionuclides by Workers. ICRP Publication 30 (Supplement to Part 1). Ann. ICRP 3 (1-4).

ICRP, 1980a. Limits for Intakes of Radionuclides by Workers. ICRP Publication 30 (Part 2). Ann. ICRP 4 (3-4).

ICRP, 1981. Limits for Intakes of Radionuclides by Workers. ICRP Publication 30 (Supplement to Part 2). Ann. ICRP 5 (1-6).

ICRP, 1990. Age-dependent Doses to Members of the Public from Intake of Radionuclides - Part 1. ICRP Publication 56. Ann. ICRP 20 (2).

ICRP, 1994. Human Respiratory Tract Model for Radiological Protection. ICRP Publication 66. Ann. ICRP 24 (1-3).

ICRP, 1993. Age Age-dependent Doses to Members of the Public from Intake of Radionuclides: Part 2 Ingestion Dose Coefficients, ICRP Publication 67. Ann. ICRP 23(3-4)

ICRP, 1994. Dose Coefficients for Intakes of Radionuclides by Workers. ICRP Publication 68. Ann. ICRP 24 (4).

ICRP, 1995a. Age-dependent Doses to Members of the Public from Intake of Radionuclides - Part 4 Inhalation Dose Coefficients. ICRP Publication 71. Ann. ICRP 25 (3-4).

ICRP, 1995b. Age-dependent Doses to the Members of the Public from Intake of Radionuclides - Part 5 Compilation of Ingestion and Inhalation Coefficients. ICRP Publication 72. Ann. ICRP 26 (1).

Kinase S, Takagi S, Noguchi H and Saito K, 2007. Application of voxel phantoms and Monte Carlo method to whole-body counter calibration Radiat. Protec. Dosim. 125(1–4), 189–93

Kramer GH and Inn KGW, 1991 A summary of the proceedings of the workshop on standard phantoms for in vivo radioactivity measurement Health Phys. 61, 893-894

Kramer G., Burns L., Guerriere S., 2002. Monte Carlo simulation of a scanning detector whole body counter and the effect of BOMAB phantom size on the calibration, Health Phys. 83(4), 526-33

Lamart, S., Blanchardon, E., Molokanov, A. et al, 2009. Study of the influence of radionuclide biokinetics on the efficiency of in vivo counting using Monte Carlo simulation. Health Phys. 96(5), 558-567

Lozano R.L,. Hernández-Ceballos M.A,. Adame J.A,. Casas-Ruiz M,. Sorribas M,. San Miguel E.G,. Bolovar J.P., 2011. Radioactive impact of Fukushima accident on the Iberian Peninsula: evolution and plume previous pathway Environ. Int. 37, 1259-1264

Masson, O., Baeza, A., Bieringer, J. et al , 2011.Tracking of airborne radionuclides from the damaged Fukushima Dai-ichi nuclear reactors by European Networks. Environ. Sci. Technol. 45 (18), 7670-7677.

Moraleda M., Gomez-Ros J., Lopez M. A., Navarro T., Navarro J. F., 2004. A MCNP-based calibration method and a voxel phantom for in vivo monitoring of 241Am in skull. Nucl. Instrum. Methods Phys. Res. A, Accel. Spectrom. Detect. Assoc. Equip 526, 551–559

McKinney G. W., Durkee J. W., Hendricks J., James M. R., Pelowitz D., Waters L. S., Gallmeiter L. X., (2006) MCNPX overview in: Proceedings of the 2006 HSSW, FNAL, IL, LA-UR-06-6206.

McKinney G. W.,. James M. R, et al., 2009. MCNPX 2.7.X - New Features Being Developed LA-UR-09-6788, IEEE/NSS Conference, Orlando, Florida, 25-31 October 2009.

Salvat F., Fernandez-Varea J. M., Sempau J., 2008. PENELOPE 2008, A Code System for Monte Carlo Simulation of Electron and Photon Transport, OECD ISBN 978-92-64-99066-1

Schläger M., 2011.Comparison of various anthropomorphic phantom types for in vivo measurements by means of Monte Carlo simulations,. Radiat. Prot. Dosim. 144(1–4), 384-388

Takahashi, M., Kinase, S., Kramer, R., 2010. Evaluation of counting efficiencies of whole-bodycounter using Monte Carlo simulation with voxel phantoms. Radiat. Prot. Dosim. 144(1-4), 407-410

Zankl, M. and Wittmann, A., 2001. The adult male voxel model ‘Golem’ segmented from whole body CT patient data. Radiat. Environ. Biophys. 40, 153–622

Zhang B., Mille M., Xu G., 2008 An analysis of dependency of counting efficiency on worker anatomy for in vivo measurements: whole-body counting. Phys. Med. Biol 53, 3463–3475